Processing of interferometric signals for a CTE measurement system

G.S. Peng and E.G. Wolff

Department of Mechanical Engineering, Oregon State University, Corvallis, OR 97331

Keywords: CTE, Michelson interferometer, fringe analysis, computer analysis

ABSTRACT

An improved Michelson interferometer and signal analysis system was developed for the CTE (coefficient of thermal expansion) measurement of thin plates and thin walled tubes. Computer based methods based on phase angle calculation to interpret the interference fringes were derived and compared to a manual chart recording approach. The computer recording system provided an automatic signal interpretation with minimal electronic circuitry. Algorithms for finding the signal phase angle were developed. Matrix operations were performed on the stored data. Requirements for signal stability and electronic noise were determined. A fixed parameter approach maps data onto a reference ellipse and eliminates the effect of ellipse size changes. Results for fused silica and composite plates and tubes in the axial direction agree well with prior work and predictions from classical composite plate theory.

INTRODUCTION

Dimensional stability is a common requirement for advanced materials and components used in aerospace applications (Blair et al., 1990) or in precision instruments. Many techniques (Hariharan, 1985; Gasvik, 1987; Smith et al., 1989) have been developed for measuring small displacements. The Michelson interferometer has been widely and successfully used in measuring the coefficient of thermal expansion (CTE) of fused silica, composite materials, and ceramics (Wolff et al, 1979; Wolff, 1987,1988). An earlier system (Wolff et al., 1985) used many optical components and complex electronic circuits to interpret the signals. Recent studies on the CTE of thin plates and thin walled tubes made from composite materials have been accompanied by improvements in instrumentation.

A single interferometer is able to measure the relative displacement of two mirrors mounted on the sample. A computer based data acquisition and analysis approach was developed to eliminate the requirement of modulating the interference signal and the fringe counting electronic circuitry (Wolff et al, 1985).

THEORY

Interference takes place when two coherent lightwaves come together at a point in space. The Michelson interferometer is one of the best known amplitude-division interference devices. The basic relationship between intensity variation and its corresponding displacement has been derived (Hecht, 1987). One can relate the displacement to the number of cycles of the intensity changes. Techniques based on digital counting were used to interpret interference fringes (Wolff et al., 1985; Sirkis, 1988). Phase angle calculation which uses two orthogonal electrical field components is another way of interpreting the signal. Figure 1 shows the decomposition of the interfered E field of an elliptical polarized light.

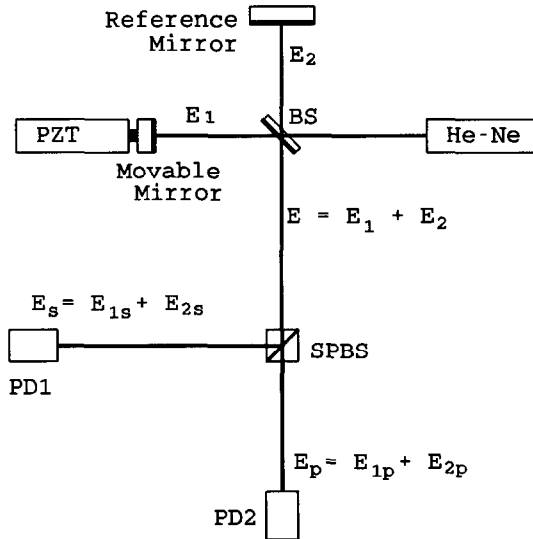Fig. 1. Decomposition of interference E field.

A linearly polarized He-Ne light is split into two beams by the 45 degrees inclined intensity beam splitter, BS. The reflected beams from the interferometer interfere upon return to this BS. The reference mirror is fixed in position while the movable mirror is moved by a PZT (piezoelectric transducer). The electrical fields of the returning beams E_1 and E_2 are separated into two orthogonal components, E_{1s}, E_{1p} and E_{2s}, E_{2p}, by a polarizing beam splitter (SPBS). There generally is a phase difference between the components of E_1 as well as between those of E_2 because of the non-coincidence between the incident beam and the principal axes of

the beamsplitter. Thus the polarization state of the recombined electrical field $\mathbf{E}$ is no longer linear but elliptical. The two orthogonal components of this elliptical polarized light after the polarizing beamsplitter can be expressed as

$$\mathbf{E}_s = \left(\mathbf{E}_{1s} + \mathbf{E}_{2s}\right) \tag{1}$$

$$\mathbf{E}_p = \left(\mathbf{E}_{1p} + \mathbf{E}_{2p}\right) \tag{2}$$

Both $\mathbf{E}_s$ and $\mathbf{E}_p$ are the resultant electrical fields of two beam interference. The corresponding irradiances of these two components are (Hecht,1987)

$$I_s = I_{1s} + I_{2s} + 2\left(I_{1s}I_{2s}\right)^{1/2}\cos\left(\phi+\delta_s\right) \tag{3}$$

$$I_p = I_{1p} + I_{2p} + 2\left(I_{1p}I_{2p}\right)^{1/2}\cos\left(\phi+\delta_p\right) \tag{4}$$

ϕ = phase difference arising from OPLD
  = $(4\pi/\lambda)nL$,
  (n, index of refraction; L, length difference between arms or sample length)
δ_s = initial phase difference between $\mathbf{E}_{1s}$ and $\mathbf{E}_{2s}$
δ_p = initial phase difference between $\mathbf{E}_{1p}$ and $\mathbf{E}_{2p}$

The first two terms of the irradiance represent the DC component while the third term is the AC part or interference term. Since we are considering the change of intensity caused by optical path length difference (OPLD), δ_s can be arbitrarily chosen, say 0, and $\delta = \delta_s - \delta_p$. Irradiance is detected by silicon photodetectors which converts the total power to a current and hence voltage. The above equations can then be written as

$$V_x = \left(V_x\right)_{DC} + \left(V_x\right)_{AC} = h + a*\cos(\phi) \tag{5}$$

$$V_y = \left(V_y\right)_{DC} + \left(V_y\right)_{AC} = k + b*\cos(\phi-\delta) \tag{6}$$

The phase angle ϕ of a given data point (V_x,V_y) can be calculated by

$$\tan\phi = \frac{\sin\phi}{\cos\phi} = \frac{\dfrac{1}{\sin\delta}\left[\dfrac{a}{b}\left(V_y-k\right) - \left(V_x-h\right)\cos\delta\right]}{\left(V_x-h\right)} \tag{7}$$

where the triangular equality $\cos(\phi-\delta) = \cos\phi\cos\delta + \sin\phi\sin\delta$ was used. The sample length change ΔL can be related to the phase angle change $\Delta\phi$ and CTE (α) as

$$\Delta L = \frac{\Delta\phi}{2kn} = \frac{\lambda}{4\pi n} \qquad \Delta\phi = L_0\alpha\Delta T \tag{8}$$

in vacuum $n = 1$, so when $\Delta\phi$ changes by 2π, ΔL will change $\lambda/2$. For a He-Ne laser, this number is 0.312 μm or 12.456 μin.

To find the parameters a, b, h, k, and δ in equation (7) for any given data point let us take the square of equations (5) and (6) and sum them up;

$$
\begin{aligned}
\frac{(V_x-h)^2}{a^2} + \frac{(V_y-k)^2}{b^2} &= \cos^2\phi + [\cos\phi\cos\delta + \sin\phi\sin\delta]^2 \\
&= \cos^2\phi + \cos^2\phi\cos^2\delta + \sin^2\phi\sin^2\delta + 2\cos\phi\cos\delta\sin\phi\sin\delta \\
&= \cos^2\phi(1+\cos^2\delta) + \sin^2\phi\sin^2\delta + 2\cos\phi\cos\delta\sin\phi\sin\delta \\
&= \cos^2\phi(\sin^2\delta +2\cos^2\delta) + \sin^2\phi\sin^2\delta + 2\cos\phi\cos\delta\sin\phi\sin\delta \\
&= \sin^2\delta(\cos^2\phi +\sin^2\phi) + 2\cos\phi\cos\delta(\cos\phi\cos\delta +\sin\phi\sin\delta) \\
&= \sin^2\delta + 2\cos\phi\cos\delta\cos(\phi-\delta) \\
&= \sin^2\delta + 2\cos\delta \frac{(V_x-h)}{a} \frac{(V_k-k)}{b}
\end{aligned}
\tag{9}
$$

We obtain the elliptical equation which represents the trajectory of the data points.

$$\frac{(V_x-h)^2}{a^2} + \frac{(V_y-k)^2}{b^2} - \frac{2(V_x-h)(V_y-k)\cos\delta}{ab} = \sin^2\delta \tag{10}$$

In this equation, (h,k) is the ellipse center. V_x ranges from h-a to h+a and V_y ranges from k-b to k+b. The initial phase difference δ between V_x and V_y determines the opening of the ellipse. Figure 2 shows an example of this equation.

To find the parameters in this equation, let us rearrange it as

$$(V_x-h)^2 + (a^2/b^2)(V_y-k)^2 - 2(a/b)(V_x-h)(V_y-k)\cos\delta = a^2\sin^2\delta \tag{11}$$

let $c = a^2/b^2$, $d = 2(a/b)\cos\delta$, $e = a^2\sin^2\delta$, $X = V_x$, $Y = V_y$

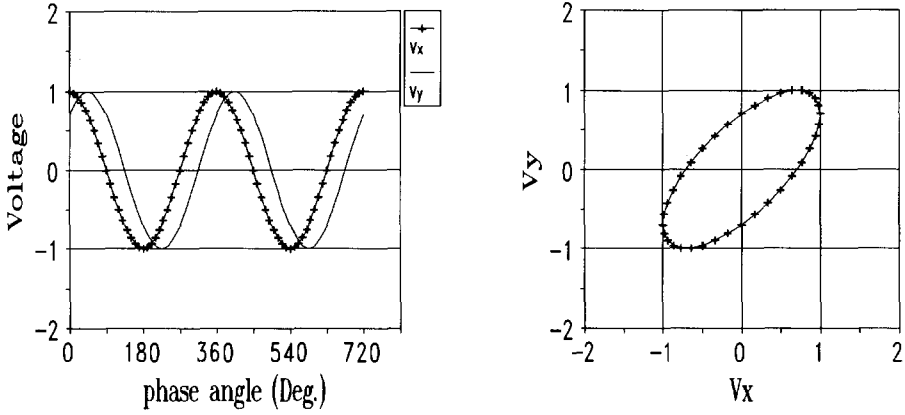Thus

$$XZ_1 - Y^2Z_2 + YZ_3 + XYZ_4 + Z_5 = X^2 \tag{12}$$

Fig. 2. (a) Simulation signal, voltage vs. phase angle, ϕ
(b) V_y vs. V_x with h = 0, k = 0, a/b = 1, δ = 45°

where $Z_1 = 2h-dk$, $Z_2 = c$, $Z_3 = 2ck-dh$, $Z_4 = d$, $Z_5 = dhk-ck^2+e$

Five data points (Vx_i,Vy_i) are read and inserted to form the equation set;

$$X_iZ_1 - Y_i^2Z_2 + Y_iZ_3 + X_iY_iZ_4 + Z_5 = X_i^2 , \quad i = 1,...,5 \tag{13}$$

Eliminate the constant term Z_5 and rewrite it in the matrix form

$$[A][Z] = [B] \tag{14}$$

where [A] and [B] are
$A(i,1) = x(1) - x(1+i)$
$A(i,2) = -(y^2(1) - y^2(1+i))$
$A(i,3) = y(1) - y(1+i)$
$A(i,4) = x(1)y(1) - x(1+i)y(1+i)$
and
$B(i) = x^2(1) - x^2(1+i)$

Once Z(i) has been solved, the parameters h, k, a/b, δ can also be found through the Z matrix as

$$h = \left(2Z_1Z_2 + Z_3Z_4\right)\Big/\left(4Z_2 - Z_4^2\right) \tag{15}$$

$$k = \left(2Z_3 + Z_1 Z_4\right)/\left(4Z_2 - Z_4^2\right) \tag{16}$$

$$a/b = \left(Z_2\right)^{1/2} \tag{17}$$

$$\cos\delta = Z_4 / \left(2\left(Z_2\right)^{1/2}\right) \tag{18}$$

The matrix operation approach finds h, k, a/b and δ after the first 5 readings. These values are then used in equation (7) to give instantaneous $\Delta L/L$ versus temperature curves.

The fixed parameters approach looks at all the V_x and V_y data stored on disk from a spreadsheet. It calculates a single set of h, k, a/b and δ parameters which are then used in equation (7) for all V_x and V_y and hence $\Delta L/L$ data.

EXPERIMENTS

Figure 3 shows the CTE measurement system. Low expansion, Al-coated glass mirrors are mounted near the opposite faces of plate samples (typically 150 mm long by 10 to 150 mm wide). Possible edge effects with composites require the mirrors to be >1 mm from any sample edge. Mirrors are aligned with another interferometer and held in place until the adhesive (Varian low-outgassing TORR-SEAL) hardens. Postcuring is recommended. For tube samples, similar mirrors are mounted on identical INVAR plates which are spring loaded against the tube ends. The laser beams in all cases are equidistant from and parallel to the plate midplane or tube axis. Cu-Constantan thermocouples (0.07 mm dia.) are attached to monitor temperature gradients.
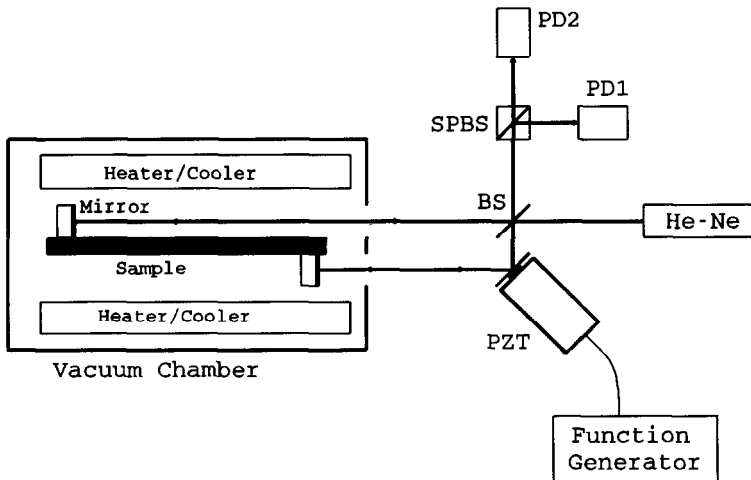
Fig. 3. CTE measurement apparatus.

Figure 4 shows that plates are supported by parallel fused silica rods and tubes are supported by vertical ZERODUR posts, all mounted on a fused silica plate. The carbon-coated copper heater/coolers are as close as possible to the samples to maximize radiative heat transfer. The cooling rate of the liquid nitrogen cooled copper can be augmented by the temporary introduction of helium into the vacuum system. However, this means temporary loss of interferometer signals. The heating is done with resistive Nichrome wires and the rate is computer controlled.

One hour drift tests are routine for system stability checks prior to heating/cooling. Figure 5 shows schematically the data acquisition system. The signal direction corresponding to sample growth or shrinkage is preset by OPLD adjustment with the PZT mounted mirror, or by temporary introduction of air, which changes the index of refraction and thus the OPLD.
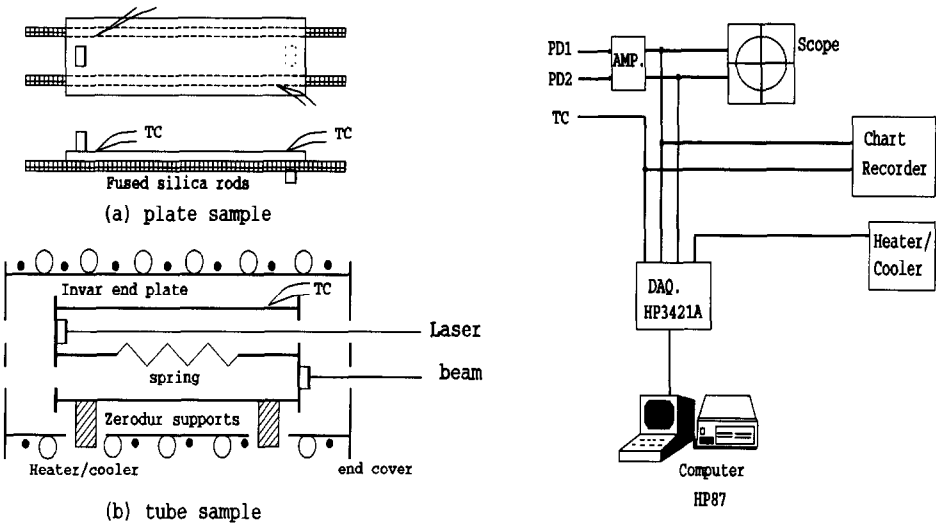
Fig. 4. CTE sample supports and heater/cooler unit
Fig. 5. Block diagram of CTE data collection system

The manual data acquisition requires only one photodetector trace and a temperature trace. One counts the number of cycles of the photodetector signal between two thermocouple readings. A PROLOG program was written to convert thermocouple reading to temperature.

Both photodetector signals were also stored on disk. A MATLAB program was written to analyze the disk data and this requires the matrix operations derived in the theory section. Thermal strain versus temperature data were then plotted from a spreadsheet such as Quattro.

The matrix operation analysis performed well except for situations where there were long periods of zero strain or temperature change or when the ellipse parameters h, k, a, b and δ were too scattered. For the fixed parameters approach, data of V_x's and V_y's such as shown in figure 2 were retrieved into a spreadsheet

to find these parameters for equation (7). The (h,k) represent the center of the ellipse and were calculated as the average of the maximum and minimum values of the X-axis and Y-axis. The amplitudes of a and b were obtained as the data range in X and Y axes, and the parameter δ was estimated to fit most of the data points. Macro commands were written in Quattro to simplify this process. These parameters were then used to obtain the phase angle of equation (7). A linear displacement of 0.6328 μm (24.91 μin.) for the simulation signal of figure 2 was obtained from both the matrix operation and fixed parameters approach. These approaches have been compared with chart recorder data for CTE measurements.

RESULTS

The CTE of a 25 mm × 100 mm × 1.6 mm thick GE type 124 fused silica plate was tested at a heating/cooling rate of 1.5°C/min. Using the chart method, the slope of the curve at room temperature was $0.49 \times 10^{-6}/°C$ as can be seen from figure 6. These results agree with similar tests on this material (Wolff et al, 1979). This experiment also showed the effect of incompletely cured adhesive holding the reflective mirrors on the sample. The first heating cycle gave a CTE value clearly too low. Subsequent work emphasized use of the proper resin to hardener ratio and adequate cure time/temperature.

Due to the relatively low thermal conductivity of fused silica, hysteresis becomes noticeable (figure 7) at a higher heating/cooling rate (3°C/min.) and the apparent slope is about $0.44 \times 10^{-6}/°C$. The same data were analyzed by computer with the fixed parameters approach. The data trajectory is shown in figure 8 and the result is shown in figure 9. It is seen that figures 7 and 9 both give a slope of $0.44 \times 10^{-6}/°C$.
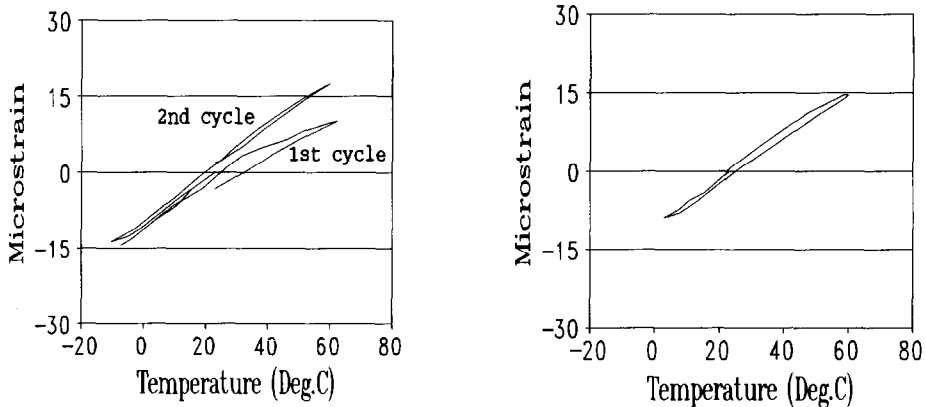

Fig. 6. Thermal strain, fused silica plate, heating/cooling rate = 1.5°C/min., chart method.
Fig. 7. Thermal strain, fused silica plate, heating/cooling rate = 3°C/min., chart method.
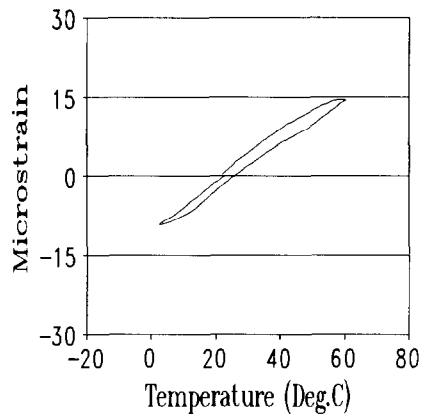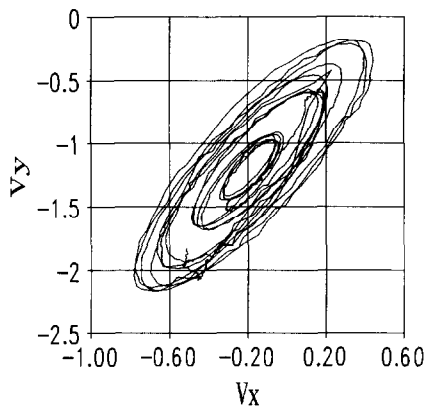
Fig. 8. Typical data trajectory, h = -0.19, k = -1.20, a/b = 0.61, δ = 32°

Fig. 9. Thermal strain, fused silica plate, heating/cooling rate = 3°C/min., fixed parameters method

A 50 mm dia. by 2.5 thick GE type 124 fused silica tube was similarly tested in the length (203 mm) direction. Figure 10 shows results are as expected, with a CTE of $0.50 \times 10^{-6}/°C$ near room temperature and $0.56 \times 10^{-6}/°C$ at 80°C.
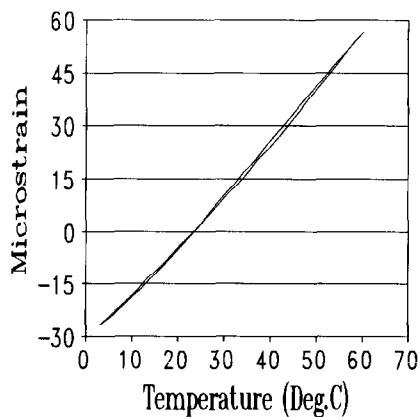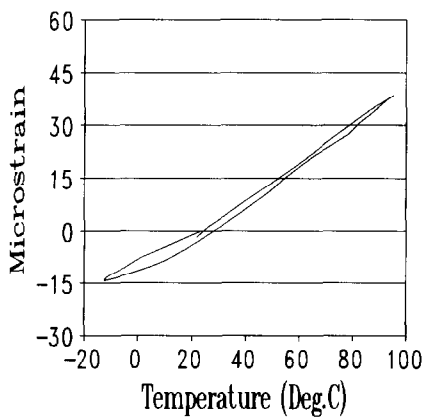

Fig. 10. Thermal strain, fused silica tube, chart method

Fig. 11. Thermal strain, composite plate, chart method

The CTE of thin composite plates (8-16 plies thick) were measured in a similar manner to the fused silica plate. Preheat just below the maximum temperature assures both complete sample dryout and mirror adhesive cure. It may also be desirable to subject the sample to a complete heating/cooling cycle prior to taking CTE data because of lower temperature microcracking effects caused by a relief of residual composite curing stresses. The greater thermal conductivity of the carbon fibers means less thermally induced hysteresis than is found with glasses, as shown in figure 11.

Figures 12 and 13 compare test results from a graphite epoxy tube, but analyzed by the fixed parameters approach in figure 12 and by the matrix operations in figure 13. The former approach is preferable since it is easier to automatically extrapolate the strain-temperature curve when the signal is temporarily lost.
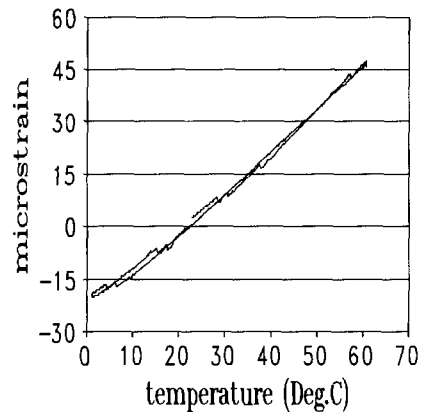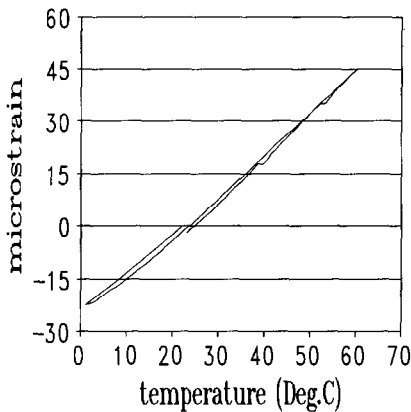
Fig. 12. Thermal strain, composite tube, fixed parameters method
Fig. 13. Thermal strain, composite tube, matrix operation method

DISCUSSION

Without automatic (remote) positioning of the sample, the signal may become lost due to excessive sample bending, bowing or twisting. (Manual realignment is accomplished with the adjustable PZT mounted mirror kept outside the vacuum system (figure 3)). Thermal gradients are the chief cause of signal loss with low thermal conductivity materials. Composite plates, however, may behave asymmetrically, even if the ply stacking sequence is mid-plane symmetric. Reasons include delaminations, microcracking, extra resin on one side, differences in surface roughness due to the mold design, and absorbed moisture, which may temporarily desorb on heating. The optics serve, to some extent, as an autocollimator to measure such out-of-plane motion. However, the beam geometry can be used to calculate both in-plane and out-of-plane motions. Since the in-plane CTE is of

primary interest, the mid-plane can also be successfully maintained parallel to the laser beams by placing a distributed vertical load on the plate sample, such as an Invar plate.

The computer analysis of the disk data requires a sufficiently high sampling rate so that the phase angle of every two points is separated by less than 180°. There is no inherent limitation to the sensitivity of the measuring system. However, the resolution of the data acquisition system determines the overall strain sensitivity.

CONCLUSION

Algorithms for analyzing interference fringes were developed and adopted to the computer based processing of CTE data on arbitrarily shaped test samples. Three methods of interference fringe analysis have been developed and compared. In each case, photodetector based signals are related to a phase angle which in turn converts to a sample displacement. These methods were: a) a manual chart recorder method, where the instantaneous V_x or V_y signals are compared to their maxima and temperature, b) a computer based approach where the average parameters of the ellipse formed by V_x and V_y (photodetector signals) are averaged (fixed) for the entire test, and c) where all these parameters are continuously updated by computer matrix operations. All these methods eliminate the need for beam modulation and considerable electronics (Wolff and Savedra, 1985). Both the manual and fixed parameters approach allow the laser beam intensity to vary arbitrarily during a CTE test, but the computer method increases analysis efficiency and accuracy. The measured phase angle depends on the ratio of the parameter a/b and not on the amplitude of the signal; thus the fixed parameters approach allows variation in laser beam intensity. This greatly reduces the need for automatic sample or beam positioning equipment (e.g., Drotning, 1982). For real time display of the thermal strain the matrix approach is used. Its accuracy increases with sampling rate and signal amplitude stability.

REFERENCES

Blair, C. and Zakrzewski, J., 1990. Coefficient of thermal and moisture expansion and moisture absorption for dimensionally stable quasi-isotropic high modulus graphite fiber/epoxy composites. *SPIE paper, Orlando Fl.*, pp. 1303-43.

Drotning, W.D., 1982. Development of a laser interferometric dilatometer. In: D.C. Larsen (editor), *Thermal Expansion 7.* Plenum Press, pp. 55-65.

Gasvik, K.J., 1987. *Optical Metrology*, Wiley.

Hariharan, P., 1985. *Optical Interferometry*, Academic Press.

Hecht, E., 1987. *Optics*, 2nd edit., Addison-Wesley Publishing, pp. 98-100 and pp. 334-336.

Sirkis, J.S. and Taylor, C.E., 1988. Interferometric-fiber-optic strain sensor. *Experimental Mechanics*, 28:170-176.

Smith, L.M. and Dobson, C.C., 1989. Absolute displacement measurements using modulation of the spectrum of white light in a Michelson interferometer. *Applied Optics*, Vol. 28, No. 15.

Wolff, E.G., 1987. Stiffness-thermal expansion relationships in high modulus carbon fibers. *Journal of Composite Materials*, 21:81-97.

Wolff, E.G., 1988.   Thermal expansion in metal/lithia-alumina-silica (LAS) composites. *International Journal of Thermophysics*, 9:221-232.

Wolff, E.G. and Eselun, S.A., 1979. Thermal expansion of a fused quartz tube in a dimensional stability facility. *Rev. Sci. Instrum.*, 50:502-506.

Wolff, E.G. and Savedra, R.C., 1985. Precision interferometric dilatometer. *Rev. Sci. Instrum.*, 56:1313-1319.